PNAS
www.pnas.org

Supplementary Information for

Mutation in *LBX1/Lbx1* precludes transcription factor cooperativity and causes congenital hypoventilation in humans and mice

Luis Rodrigo Hernandez-Miranda, Daniel M. Ibrahim, Pierre-Louis Ruffault, Madeleine Larrosa, Kira Balueva, Thomas Müller, Willemien de Weerd, Irene Stolte-Dijkstra, Robert MW Hostra, Jean-François Brunet, Gilles Fortin, Stefan Mundlos and Carmen Birchmeier

Correspondence to Carmen Birchmeier
Email: cbirch@mdc-berlin.de

This PDF file includes:

www.pnas.org/cgi/doi/10.1073/pnas.1813520115

Supplementary Information Text

SI Materials and Methods

Animals. All animal experimental procedures were done in accordance to the guidance and policies of the Max-Delbrueck-Centrum fuer Molekulare Medizin, Berlin, Germany; the Institut des Neurosciences Paris-Saclay, Gif-sur-Yvette, France; and the Max Planck Institute for Molecular Genetics, Berlin, Germany. Mouse strains used for this study were: Ai65 (1), $Egr2^{cre}$ (2), $Lbx1^{cre}$ (3), $Lbx1^{null}$ (4); and $Phox2b^{Flpo}$ (5). All strains were maintained in a mixed genetic background.

Generation of $Lbx1^{lox}$ and $Lbx1^{FS}$ transgenic mouse strains. A 144-kb BAC clone RP23–188J8 (RZPD, Berlin, Germany) containing Lbx1 was modified using homologous recombination in bacteria as described (6). For *$Lbx1^{lox}$* mice, one loxP site and a neo-cassette flanked by FRT sites were inserted into the intron between exon 1 and 2, and the second loxP site and a SpeI recombination site were inserted downstream of exon 2. For *$Lbx1^{FS}$* mice, the corresponding mouse sequence was replaced by the human exon 2 sequence containing the frameshift mutation. A neo-cassette flanked by FRT sites was inserted into the intron, and a SpeI site was introduced downstream of exon 2. Mutant alleles were generated by homologous recombination in ES cells, and mice containing the mutant allele were derived by blastocyst injection. The neo-cassettes were removed in mice by Flp-recombination in the germline using the Flp-deleter strain (7).

removed in mice by Flp-recombination in the germline using the Flp-deleter strain (7).

Clinical presentation of the LBX$^{FS/FS}$ patients. The children studied here (V:2, V:3), demonstrated an autosomal recessive pattern of alveolar hypoventilation in the neonatal period. In addition to the respiratory phenotype described, both probands presented paroxysmal attacks of hypertension with pallor and sweating. There was no baseline brachycardia or transient asystole. During the first years of life the two children had frequent feeding problems, recurrent vomiting, diarrhea and prolonged periods of constipations. Profound heat intolerance was observed in both siblings, with inordinate high (42°C) and low (34°C) temperatures present during infections.

Plethysmography. Unrestrained whole body plethysmography was performed as described (8). Because of the severe breathing deficits, litters containing *Lbx1*$^{FS/FS}$ and *dB2-Lbx1*^{FS} mice were delivered by Caesarian sections; litters containing *Egr2-Lbx1*^{FS} animals that are less severely affected were delivered by natural birth. For the plethysmography, the animals were individually placed in a 20 ml Plexiglas chamber hermetically closed and connected to a Validyne (model DP103-10; California, USA) pressure transducer and to a reference chamber of equal volume. The pressure difference between the two chambers was measured with a pressure transducer (Validyne, DP 103–14) connected to a sine wave carrier demodulator (Validyne, CD15). The spirogram was acquired at a

sampling frequency of 1 kHz and was stored on a computer using a labmaster interface. Calibrations were recorded at the end of each recording session by injecting a defined volume of air (1–5 µl) into the test chamber using a Hamilton syringe. Plethysmographic recordings were analyzed on Elphy software (developed by G Sadoc at CNRS, Gif-sur-Yvette, France). A plethysmographic session per animal lasted five minutes. For CO_2 challenges, a gas mixture composed of 8% CO_2, 21% O_2 and 71% N_2 was applied into the chamber for a three minute period as described (9).

Calcium imaging. Calcium imaging experiments were performed as described (10). In short, whole-mount brainstem or slice preparations were dissected and incubated at room temperature for 40–45 min in oxygenated artificial cerebrospinal fluid containing the cell-permeant calcium indicator dye Calcium Green-1 AM (10 µM; Life Technologies, Paisley, UK). Preparations were then transferred to a recording chamber (30°C) and let to recover for 30 min prior to the start of optical recordings. Optical recordings were done using a conventional epifluorescence microscope with a FITC filter cube. Fluorescence images were captured with a cooled Neo sCMOS camera (Andor Technology Ltd., Belfast, UK) using 10×, 20× and 40× objectives, an exposure time of 100ms and bin size of 4 × 4 for periods of 180s using Micro-Manager software (https://www.micro-manager.org/wiki/).

Histology and cell quantifications. Cell quantifications were performed on consecutive 20μm transverse sections encompassing rhombomere 1-7. Immunofluorescence, *in situ* hybridization and tissue processing were performed as described (11). The following antibodies were used: goat anti-ChAT (Millipore, Temecula, USA), rabbit anti-Phox2b (12), guinea pig anti-Lbx1 (13), rat anti-BrdU (Abcam, Cambridge, UK), goat anti-Foxp2 (Abcam), rabbit anti-RFP (Abcam), rabbit anti-Pax2 (Millipore), guinea pig anti-Lmx1b (13), chicken anti-laminin (Abcam), goat anti-desmin (R&D Systems, Minneapolis, MN). Primer sequences to generate *in situ* probes for *Atoh1* and for *Somatostatin* (*SST*) were obtained from the Allen Brain Atlas website. For pulse labeling, BrdU (2mg) was injected into pregnant dams at gestational day 11.5, and the animals were sacrificed 30 minutes after the injection. Fluorescencent microphotographs were acquired on a Zeiss LSM 700 confocal microcope in a non-blind manner. Unless otherwise specified, the confocal tile scan modus was used to acquire photomicrographs, and assembled using ZEN2012 software with a 10% overlap between tiles.

Cell cultures. P19 murine embryonic teracarcinoma cells were obtained from ATTC (CRL-1825™) and differentiated into neurons using 1 μM retinoic acid (Sigma) as described (14). Briefly, P19 cell suspension cultures were incubated for 4 days in neuronal differentiation media (94%DMEM, 5% FBS, 1% Pep/Strep and 1 μM retinoic acid) to allow for the formation of embryoid bodies. The embryoid bodies were treated with trypsin on the fourth day of differentiation and plated as a monolayer on laminin (10mg/ml) coated dishes for terminal neuronal

differentiation. Cytosine β-D-arabinoside (AraC, 12μM; Sigma) was added to the differentiation media on the sixth day to eliminate proliferative cells and enrich for postmitotic neurons. Neurons were collected for chromatin and RNA extraction on the seventh day of differentiation.

CRISPR-Cas9 deletion of Lbx1 in P19 cells and generation of cell lines. For generation of *Lbx1* mutant cells, two distinct sgRNAs were designed using the free online CRIPR-Cas9 tool (http://crispr.mit.edu; sequences are listed in Supplementary Table 1) and cloned into a px330 CRISPR-Cas9-Cherry vector. Vectors were transfected into undifferentiated P19 cells using Lipofectamine 2000 (Sigma), and cells were isolated by fluorescent activated cell sorting. Western blotting using Lbx1 antibodies and Sanger sequencing were carried out to identify *Lbx1* mutant clones. *Lbx1* mutant cells were transduced with pMCs-puro-Retroviral (Cell Biolabs, Inc; San Diego, USA) vectors encoding $Lbx1^{flag}$, $Lbx1FS^{flag}$ and $Phox2b^{HA}$. Retroviruses containing a 2A sequence between the Lbx1 and Phox2b sequences were used to generate Lbx1/Phox2b and $Lbx1^{FS}$/Phox2b expressing cells.

Chromatin-immunoprecipitation (ChIP) and next generation sequencing. Mouse anti-Flag (Sigma; to detect Lbx1/$Lbx1^{FS}$), mouse anti-HA (Sigma; to detect Phox2b), rabbit anti-H3K27ac (Invitrogen) and rabbit anti-H3K27me3 (Invitrogene) were used for chromatin immunoprecipitation. Chromatin was prepared from differentiated P19 neuronal cultures as described (15, 16).

Immunoprecipitated DNA was used for qPCR or next generation sequencing downstream analyses. Primers for qPCR analysis are listed in Supplementary Table 1. For next generation sequencing, Lbx1 and Lbx1^{FS} immuno-precipitated DNA was used to prepare Illumina (Illumina, San Diego, USA) libraries as described (15, 16). In brief, the following preparation steps were performed to create a library for each sample: end-repair, A-tailing, adapter ligation, gel purification and a final PCR enrichment. After quality control on an Agilent Bioanalyzer and quantification of final libraries on Qubit, cluster generation and sequencing were conducted. The ChIP-seq library was sequenced on single-end 50bp using Illumina technology. The data were visualized using the UCSC genome browser (https://genome.ucsc.edu).

RNA extraction and next generation sequencing. Total RNA from P19 cells was extracted using Trizol-based protocols. RNA samples were DNase treated using the DNA-free DNA Removal Kit (Thermo Fisher Scientific; MA, USA) and analyzed on Agilent (California, USA) Bioanalyzer 2100 using the Agilent RNA 6000 Nano Kit. Primers for qPCR quantification of *Lbx1*, *Lmx1b*, *Prrxl1* and *Pou4f1* are listed in Supplementary Table 1. For RNA sequencing, strand-specific cDNA libraries were generated according to the Illumina TruSeq protocol (TruSeq Stranded mRNA LT Sample Prep Kit). The libraries were sequenced on an Illumina NextSeq 500 System, using High Output Kit, 1x 150 cycles.

Computational analyses of Chip-seq data: Mapping, peak calling, and quality control. For each biological replicate, raw ChIP-seq reads were mapped to mm9 using bowtie2 (PARAMETERS) and only unique matches were retained. Efficiency of enrichment was evaluated using SPP cross-correlation analysis for each replicate independently. Peaks for each were called using the Q peak caller (PARAMETERS) and Input chromatin as control. To identify reproducible binding sites IDR analysis was performed and reproducible peaks with an irreproducible discovery rate (IDR) >0.1 were kept as reproducible binding sites for the respective transcription factor. **Binding visualization and overlaps.** For visualization, each read was extended to 250bp (mean sonication size) and a bigwig track of coverage normalized reads per million was created using bedtools' genomecoveragebed and UCSC's bedgraphtobigwig tools (17). Overlapping peaks were identified using bedtools (18). **Motif Analysis.** *De novo* motif analysis was performed for all reproducible binding sites using RSAT (19) and its positions algorithm. **Read Enrichment Analysis.** Analysis was performed using seqMINER (20). For each experiment generate a subsampled bam file with 40Mio randomly selected reads and computed the enrichment for all sites bound by either Lbx1 or Lbx1FS. This was then used to perform k-means clustering (raw) with 10 expected clusters. All heatmaps are +/- 5kb. **RNA-seq analysis.** Paired-end reads were mapped to the murine reference genome (mm9) using the STAR mapper (splice junctions based on RefSeq; options: --alignIntronMin 20 --alignIntronMax 500000 --outFilterMultimapNmax 5 --outFilterMismatchNmax 10 --outFilterMismatchNoverLmax 0.1) (21). Reads per

gene were counted as described previously and used for differential expression analysis with the DEseq2 package (22, 23).

Statistics. Statistical analyses were performed using the software Prism 7 (GraphPad). All data are plotted in box plots with median, quartiles (boxes) and ranges (whiskers). The statistical significance between group means was tested by one-way ANOVA, followed by Bonferroni's *post hoc* test (for multiple-comparison tests), or two-end t-test (for pair comparison tests). Degrees of Freedom as well as F and t values are provided in each figure legend. To determine statistical significance of the breathing behavior among distinct groups studied, the distribution of the plethysmographic data was first assessed by a D'Agostino & Pearson omnibus normality test and group mean significance was subsequently estimated by a non-parametric Mann-Whitney U test.

References for SI Materials and Methods

1. Madisen L*, et al.* (2015) Transgenic mice for intersectional targeting of neural sensors and effectors with high specificity and performance. *Neuron* 85(5):942-958.

2. Voiculescu O, Charnay P, & Schneider-Maunoury S (2000) Expression pattern of a Krox-20/Cre knock-in allele in the developing hindbrain, bones, and peripheral nervous system. *Genesis* 26(2):123-126.

3. Vasyutina E*, et al.* (2007) RBP-J (Rbpsuh) is essential to maintain muscle progenitor cells and to generate satellite cells. *Proc Natl Acad Sci U S A* 104(11):4443-4448.

4. Brohmann H, Jagla K, & Birchmeier C (2000) The role of Lbx1 in migration of muscle precursor cells. *Development* 127(2):437-445.

5. Hirsch MR, d'Autreaux F, Dymecki SM, Brunet JF, & Goridis C (2013) A Phox2b::FLPo transgenic mouse line suitable for intersectional genetics. *Genesis* 51(7):506-514.

6. Sieber MA*, et al.* (2007) Lbx1 acts as a selector gene in the fate determination of somatosensory and viscerosensory relay neurons in the hindbrain. *J Neurosci* 27(18):4902-4909.

7. Farley FW, Soriano P, Steffen LS, & Dymecki SM (2000) Widespread recombinase expression using FLPeR (flipper) mice. *Genesis* 28(3-4):106-110.

8. Hernandez-Miranda LR*, et al.* (2017) Genetic identification of a hindbrain nucleus essential for innate vocalization. *Proc Natl Acad Sci U S A* 114(30):8095-8100.

9. Spielmann M*, et al.* (2017) Mutations in MYO1H cause a recessive form of central hypoventilation with autonomic dysfunction. *J Med Genet* 54(11):754-761.

10. Bouvier J*, et al.* (2010) Hindbrain interneurons and axon guidance signaling critical for breathing. *Nat Neurosci* 13(9):1066-1074.

11. Hernandez-Miranda LR*, et al.* (2011) Robo1 regulates semaphorin signaling to guide the migration of cortical interneurons through the ventral forebrain. *J Neurosci* 31(16):6174-6187.

12. Dauger S*, et al.* (2003) Phox2b controls the development of peripheral chemoreceptors and afferent visceral pathways. *Development* 130(26):6635-6642.

13. Muller T*, et al.* (2002) The homeodomain factor lbx1 distinguishes two major programs of neuronal differentiation in the dorsal spinal cord. *Neuron* 34(4):551-562.

14. Monzo HJ*, et al.* (2012) A method for generating high-yield enriched neuronal cultures from P19 embryonal carcinoma cells. *J Neurosci Methods* 204(1):87-103.

15. Ibrahim DM*, et al.* (2013) Distinct global shifts in genomic binding profiles of limb malformation-associated HOXD13 mutations. *Genome Res* 23(12):2091-2102.

16. Jia S*, et al.* (2015) Insm1 cooperates with Neurod1 and Foxa2 to maintain mature pancreatic beta-cell function. *EMBO J* 34(10):1417-1433.

17. Kent WJ, Zweig AS, Barber G, Hinrichs AS, & Karolchik D (2010) BigWig and BigBed: enabling browsing of large distributed datasets. *Bioinformatics* 26(17):2204-2207.

18. Quinlan AR (2014) BEDTools: The Swiss-Army Tool for Genome Feature Analysis. *Curr Protoc Bioinformatics* 47:11 12 11-34.

19. Medina-Rivera A*, et al.* (2015) RSAT 2015: Regulatory Sequence Analysis Tools. *Nucleic Acids Res* 43(W1):W50-56.

20. Ye T*, et al.* (2011) seqMINER: an integrated ChIP-seq data interpretation platform. *Nucleic Acids Res* 39(6):e35.

21. Dobin A*, et al.* (2013) STAR: ultrafast universal RNA-seq aligner. *Bioinformatics* 29(1):15-21.

22. Franke M*, et al.* (2016) Formation of new chromatin domains determines pathogenicity of genomic duplications. *Nature* 538(7624):265-269.

23. Love MI, Huber W, & Anders S (2014) Moderated estimation of fold change and dispersion for RNA-seq data with DESeq2. *Genome Biol* 15(12):550.

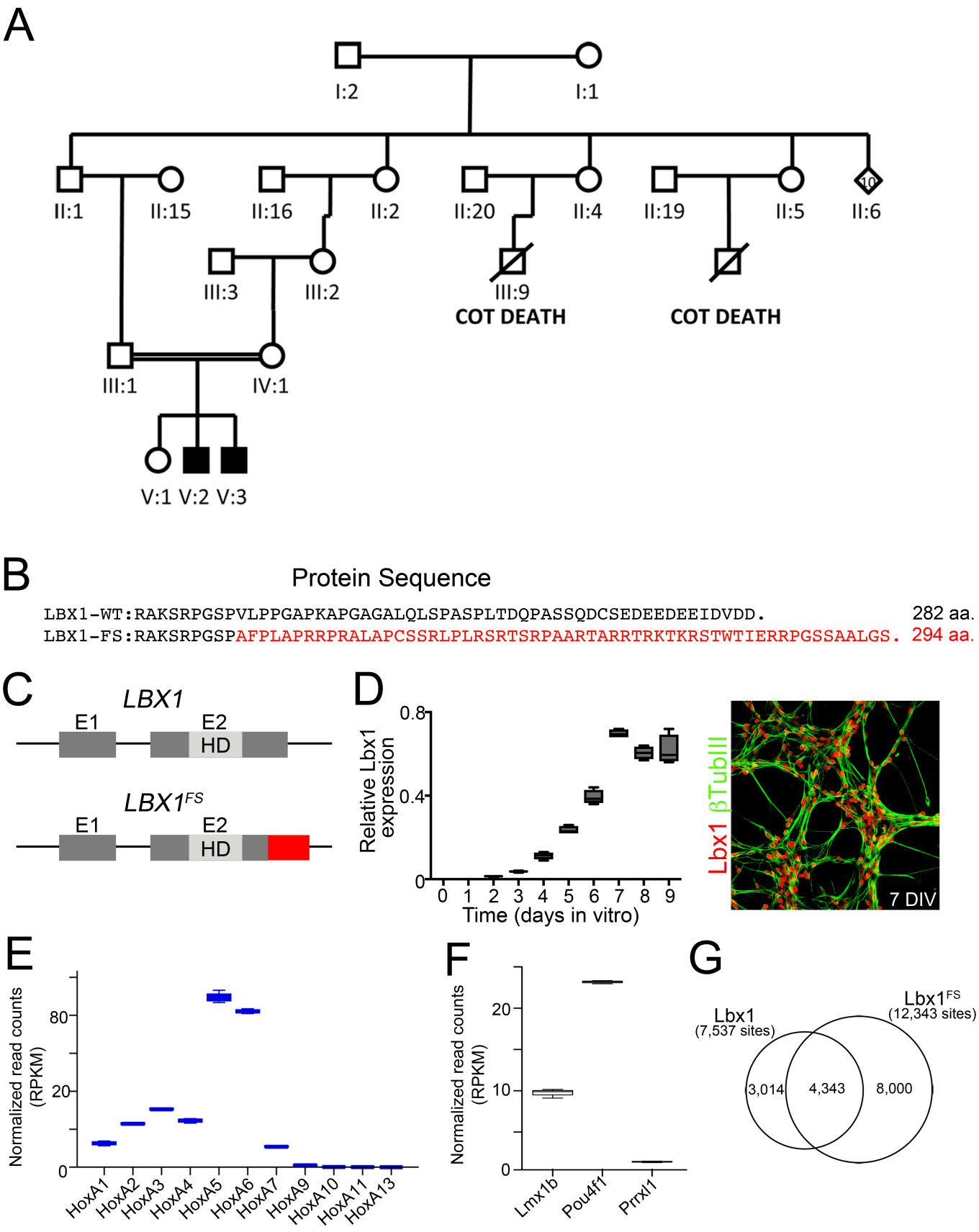
A
I:2
I:1
II:1
II:15
II:16
II:2
II:20
II:4
II:19
II:5
II:6
III:3
III:2
III:9
COT DEATH
COT DEATH
III:1
IV:1
V:1 V:2 V:3
B
Protein Sequence
LBX1-WT:RAKSRPGSPVLPPGAPKAPGAGALQLSPASPLTDQPASSQDCSEDEEDEEIDVDD. 282 aa.
LBX1-FS:RAKSRPGSPAFPLAPRRPRALAPCSSRLPLRSRTSRPAARTARRTRKTKRSTWTIERRPGSSAALGS. 294 aa.
C
LBX1
E1
E2
HD
LBX1FS
E1
E2
HD
D
Relative Lbx1 expression
0.8
0.4
0
0 1 2 3 4 5 6 7 8 9
Time (days in vitro)
Lbx1 βTubIII
7 DIV
E
Normalized read counts (RPKM)
80
20
0
HoxA1
HoxA2
HoxA3
HoxA4
HoxA5
HoxA6
HoxA7
HoxA9
HoxA10
HoxA11
HoxA13
F
Normalized read counts (RPKM)
20
10
0
Lmx1b
Pou4f1
Prrxl1
G
Lbx1
(7,537 sites)
Lbx1FS
(12,343 sites)
3,014
4,343
8,000

Fig. S1

Fig. S1. The identified frameshift mutation in *Lbx1* affects the C-terminus of the protein. (**A**) Extended pedigree of a family with two children diagnosed with CCHS (black). (**B**) C-terminus protein sequence of LBX1 (wildtype) and LBX1^{FS} proteins. (**C**) (Top) The wildtype *LBX1* gene contains two exons and encodes a homeodomain transcription factor. The homeodomain coding sequence is marked (HD). (Bottom) The identified *LBX1* frameshift (*LBX1^{FS}*) mutation alters the C-terminus protein coding sequence (indicated in red). (**D**) (Left) qPCR analysis of *Lbx1* expression in wildtype P19 cells during neuronal differentiation. (Right) Histological analysis of P19 cells with antibodies against Lbx1 (red) and the neuronal marker β-tubulin III (green) seven days after induction of differentiation (DIV). (**E**) Normalized read counts for various *HoxA* gene transcripts in neurons differentiated from P19 cells that endogenously express Lbx1 (n=3 independent replicates). (**F**) Normalized read counts for transcripts of the somatosensory genes Lmx1b, Prrxl1 and Pou4f1 in neurons differentiated from P19 cells (n=3 independent replicates). (**G**) Venn diagram illustrating the overlap of Lbx1 and Lbx1^{FS} genome-wide binding sites.

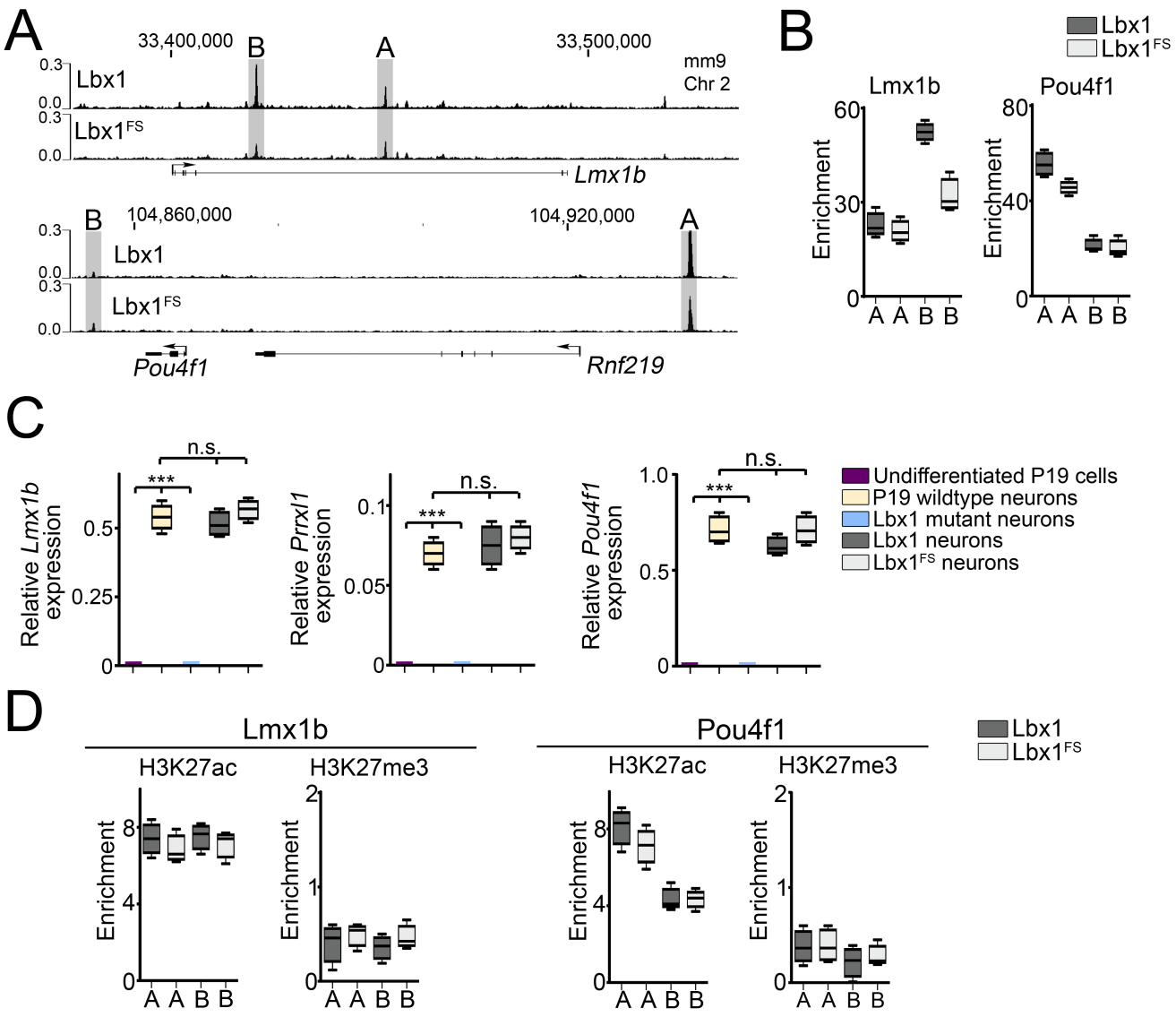
A
33,400,000
B
A
33,500,000
mm9
Chr 2
Lbx1
Lbx1FS
Lmx1b
104,860,000
104,920,000
Pou4f1
Rnf219
B
Lbx1
Lbx1FS
Lmx1b
Pou4f1
Enrichment
A A B B
C
Relative Lmx1b expression
Relative Prrxl1 expression
Relative Pou4f1 expression
n.s.
***
Undifferentiated P19 cells
P19 wildtype neurons
Lbx1 mutant neurons
Lbx1 neurons
Lbx1FS neurons
D
Lmx1b
Pou4f1
H3K27ac
H3K27me3
Enrichment
Lbx1
Lbx1FS

Fig. S2

Fig. S2. Genome-wide analysis demonstrates similarities of Lbx1 and Lbx1^{FS} binding in regulatory sequences of somatosensory genes. (**A**) ChIP-seq tracks illustrating Lbx1 and Lbx1^{FS} occupancy on intergenic and intronic regions of *Lmx1b* and *Pou4f1* loci. Selected regions for ChIP-qPCR analysis are indicated in gray. (**B**) ChIP-qPCR analysis of Lbx1 and Lbx1^{FS} occupancy on the gray highlighted regions of *Lmx1b* and *Pou4f1* displayed in A (n=4 independent duplicates). (**C**) qPCR analysis (n=3 independent replicates) of *Lmx1b* (one-way ANOVA, F(4, 15)=287,7), *Prrxl1* (one-way ANOVA, F(4, 15)=113,3) and *Pou4f1* (one-way ANOVA, F(4, 15)=205,3) expression in neurons differentiated from wildtype P19 cells that express *Lbx1* endogenously (P19 neurons), P19 *Lbx1* mutant neurons, and transduced P19 *Lbx1* mutant cells with flag-tagged Lbx1 and flag-tagged Lbx1^{FS} (for simplicity Lbx1 and Lbx1^{FS} neurons). (**D**) H3K27ac and H3K27me3 ChIP-qPCR analysis performed on chromatin prepared from Lbx1 and Lbx1^{FS} differentiated neurons (n=4 independent duplicates) on the selected regions displayed in A. ***P < 0.0001.

A

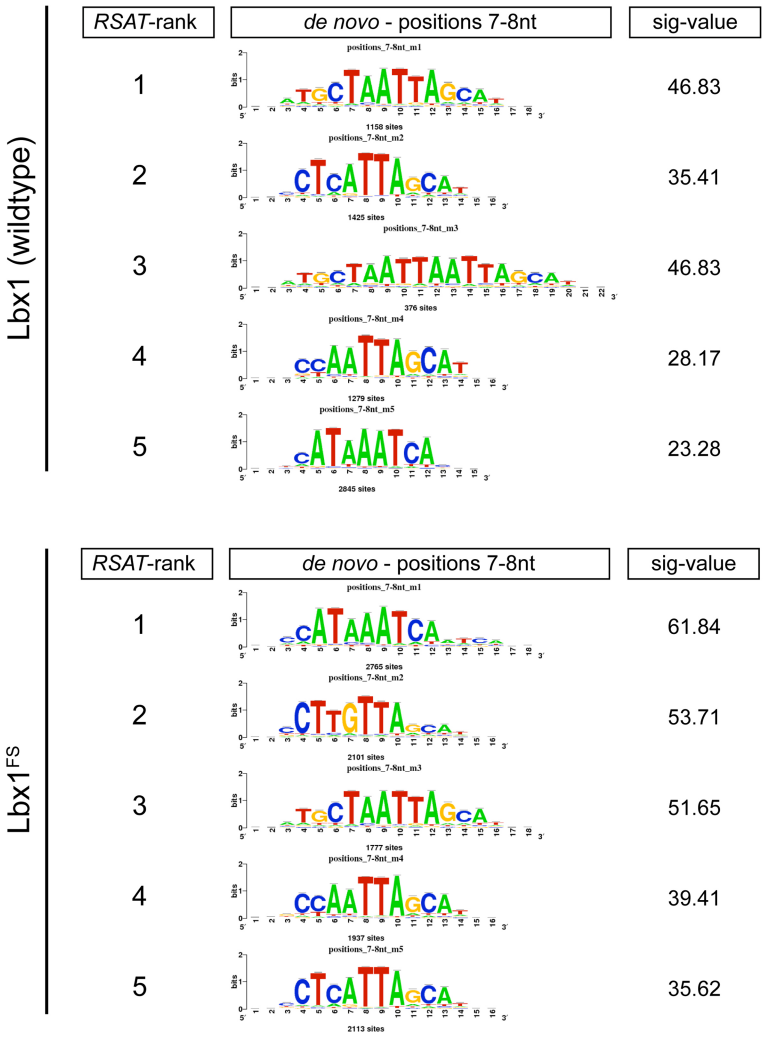

B

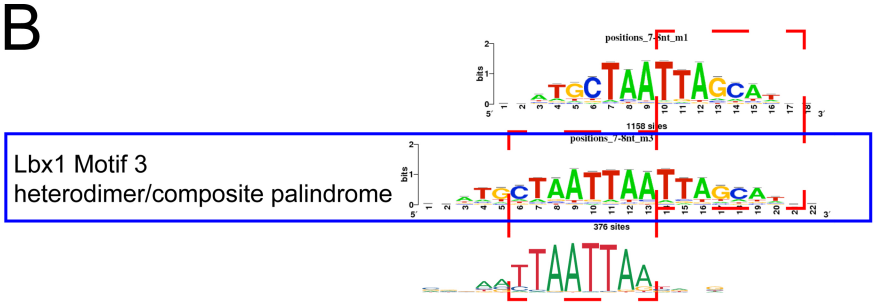

Lbx1 Motif1 homodimer palindrome

Phox2b site (JASPAR PH0136.1)

Fig. S3

Fig. S3. *de novo* motif analysis of Lbx1 and Lbx1^{FS} binding sequence preferences. (**A**) Most frequent motif sequences identified in Lbx1 and Lbx1^{FS} binding sites. (**B**) The third most frequent motif sequence (blue rectangle) identified in Lbx1 binding sites is composed of Lbx1 (top) and Phox2b (bottom) monomer sequences.

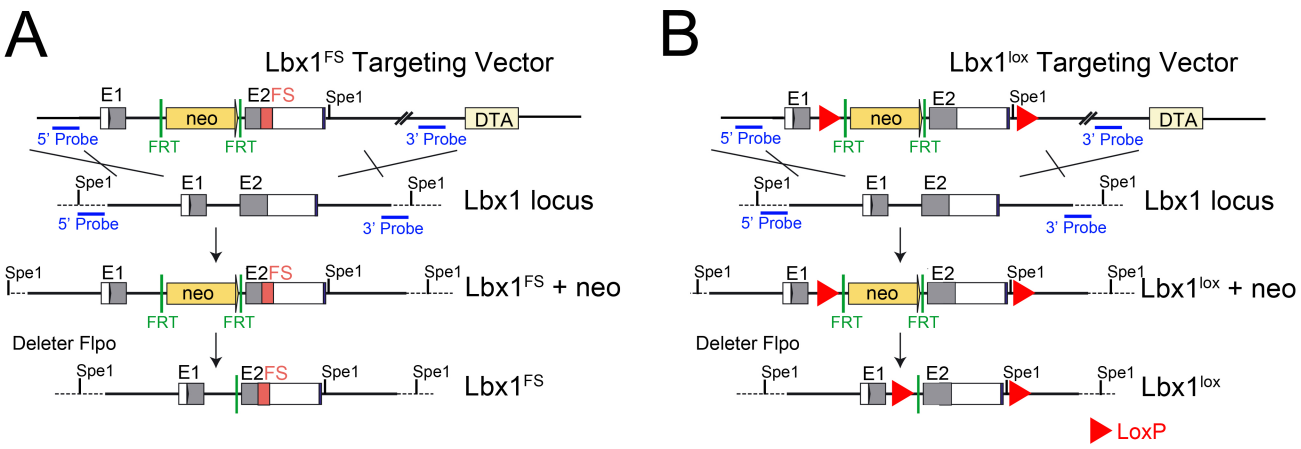
A
Lbx1FS Targeting Vector
E1
neo
E2FS
Spe1
DTA
5' Probe
FRT
FRT
3' Probe
Spe1
E1
E2
Spe1
Lbx1 locus
5' Probe
3' Probe
Spe1
E1
neo
E2FS
Spe1
Spe1
Lbx1FS + neo
FRT
FRT
Deleter Flpo
Spe1
E1
E2FS
Spe1
Spe1
Lbx1FS
B
Lbx1lox Targeting Vector
E1
neo
E2
Spe1
DTA
5' Probe
FRT
FRT
3' Probe
Spe1
E1
E2
Spe1
Lbx1 locus
5' Probe
3' Probe
Spe1
E1
neo
E2
Spe1
Spe1
Lbx1lox + neo
FRT
FRT
Deleter Flpo
Spe1
E1
E2
Spe1
Spe1
Lbx1lox
LoxP

Fig. S4

Fig. S4. Generation of the *Lbx1*^{FS} and *Lbx1*^{lox} mouse strains. Schematic representation of the targeting vector used to introduce the *Lbx1*^{FS} (**A**) and *Lbx1*^{lox} (**B**) mutations into the wildtype *Lbx1* locus by homologous recombination in embryonic stem cells. The neomycin (Neo) resistance cassettes used for selection of ES cells were removed using a deleter Flpo strain (see SI Appendix, Materials and Methods).

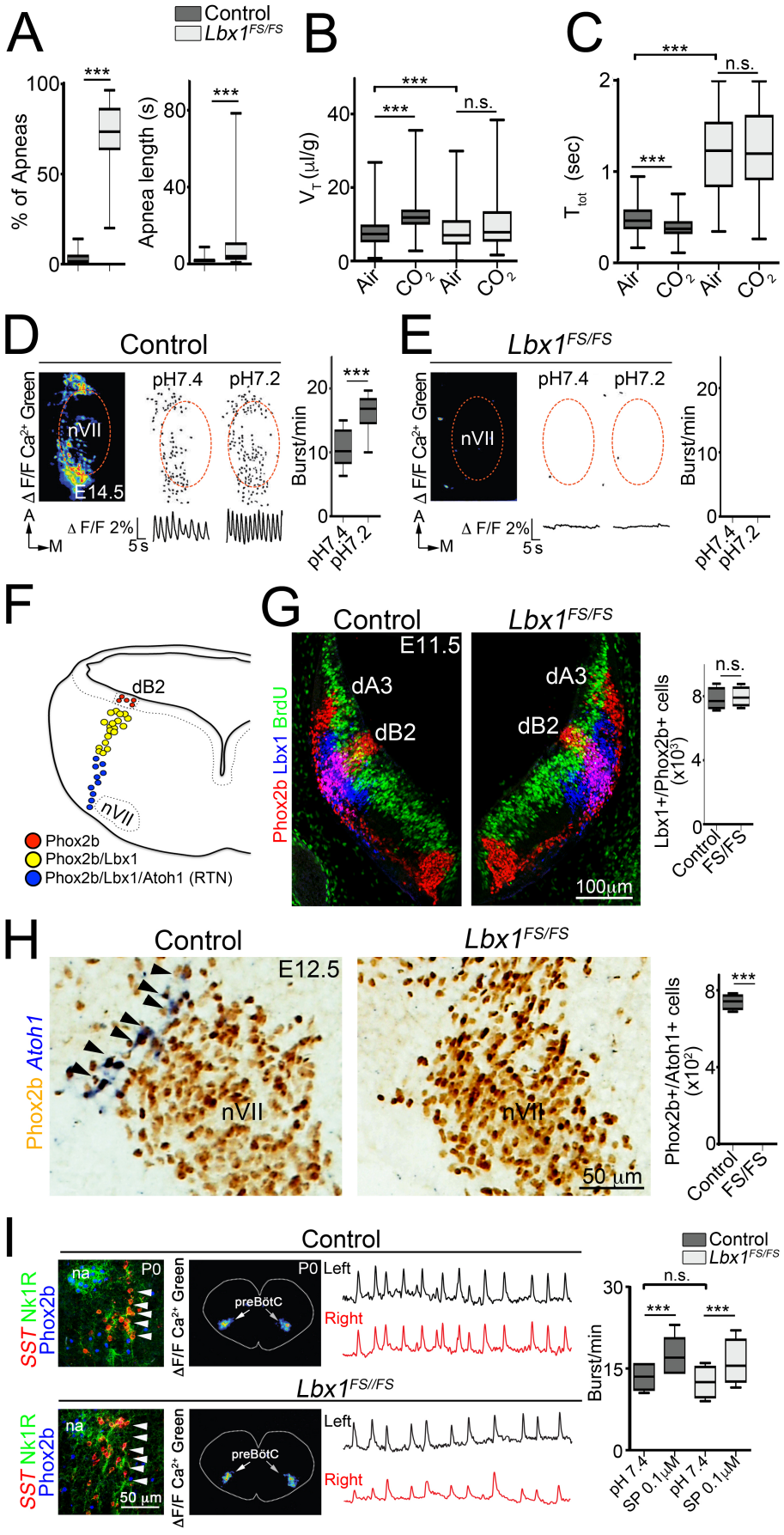
A
Control
Lbx1FS/FS
% of Apneas
Apnea length (s)
B
VT (µl/g)
Air
CO2
C
Ttot (sec)
n.s.
D
Control
ΔF/F Ca2+ Green
nVII
E14.5
pH7.4
pH7.2
Burst/min
ΔF/F 2%
5s
E
Lbx1FS/FS
F
dB2
nVII
Phox2b
Phox2b/Lbx1
Phox2b/Lbx1/Atoh1 (RTN)
G
Control
Lbx1FS/FS
E11.5
dA3
dB2
Phox2b Lbx1 BrdU
100µm
Lbx1+/Phox2b+ cells (x10³)
Control
FS/FS
H
Control
Lbx1FS/FS
E12.5
Phox2b Atoh1
50 µm
Phox2b+/Atoh1+ cells (x10²)
I
Control
Lbx1FS/FS
SST Nk1R Phox2b
na
P0
preBötC
ΔF/F Ca2+ Green
Left
Right
Lbx1FS//FS
Burst/min
pH 7.4
SP 0.1µM

Fig. S5

Fig. S5. *Lbx1*^{FS} mice failed to respond to high levels of CO_2 in air. (**A-C**) Breathing analysis of control (n=9) and *Lbx1*$^{FS/FS}$ (n=11) newborn mice. (**A**) (Left) Quantification of the percentage of apneic episodes (per 5-minute breathing recordings; unpaired non-parametric Mann-Whitney U test). (Right) Quantification of apnea lengths (per 5-minute breathing recordings; unpaired non-parametric Mann-Whitney U test). (**B**) Quantification of tidal volumes (V_T; unpaired non-parametric Mann-Whitney U test) of control and *Lbx1*$^{FS/FS}$ newborns in normal air and in high CO_2 containing air. (**C**) Quantification of breath cycle duration (T_{TOT}; unpaired non-parametric Mann-Whitney U test) of control and *Lbx1*$^{FS/FS}$ newborns in normal air and in high CO_2 containing air. (**D**) (Left) Ventral hindbrain view centered on the facial (nVII) motor nucleus (dotted) showing Ca^{2+} green-1AM fluorescence changes (ΔF/F) of RTN cells in an E14.5 control brainstem preparation. RTN cell activity maps (top) and average population activity traces (bottom) at pH7.4 and pH7.2. Note that from a ventral view, RTN cells seem to localize on top of the facial motor nucleus. (Right) Quantification of RTN activity (bursts/minute) at pH7.4 and pH7.2 (n=12; unpaired t test, t=4,872, df=22). **(E)** Corresponding maps, tracings and quantifications of RTN activity of E14.5 *Lbx1*$^{FS/FS}$ embryos demonstrating the absence of a functional RTN (n=5). (**F**) Scheme illustrating RTN neuron development. Phox2b+ progenitors (red) generate Lbx1+/Phox2b+ dB2 neurons (yellow). A subpopulation of dB2 cells migrates ventrally, initiates *Atoh1* expression and matures into RTN neurons (blue). The location of the facial motor nucleus (nVII) is indicated. (**G**) (Left and middle) Histological analysis of dB2

(magenta) neurons that co-express Lbx1 (blue) and Phox2b (red) in control and *Lbx1*$^{FS/FS}$ embryos at E11.5. A pulse labeling with BrdU (green) was used to delineate proliferating progenitors; note that dB2 neurons are BrdU negative, i.e. postmitotic. Confocal tile scan modus was used to acquire photomicrographs, and assembled using ZEN2012 software (10% overlap between tiles). (Right), quantification of Lbx1+/Phox2b+ dB2 neurons in control and *Lbx1*$^{FS/FS}$ embryos at E11.5 (n=4 per condition; unpaired t test, t=0,2917, df=6). (**H**) (Left and middle) Histological analysis of migrating Atoh1+ (blue) and Phox2b+ (brown) dB2 neurons (arrowheads) in control and *Lbx1*$^{FS/FS}$ embryos at E12.5. (Right) quantification of Phox2b+/Atoh1+ dB2 neurons in control (n=4) and *Lbx1*$^{FS/FS}$ (n=4) embryos at E12.5 (unpaired t test, t=34,35 df=6). (**I**) (Left) Analysis of the preBötzinger complex in control and *Lbx1*$^{FS/FS}$ newborns by histology using antibodies against Neurokinin 1 receptor (Nk1R; green) and an *in situ* probe against somatostatin (SST, red); Phox2b (blue) and Nk1R antibodies mark the nucleus ambiguus. (Middle) Analysis of the activity of the preBötzinger complex by Ca^{2+} imaging of control and *Lbx1*$^{FS/FS}$ mice at P0. (Right) The preBötzinger complex activity is similar in control and *Lbx1*$^{FS/FS}$ mice at pH 7.4 and in response to 0.1 μM substance P (SP) (one-way ANOVA, F(3, 16)=2,476). ***P < 0.0001.

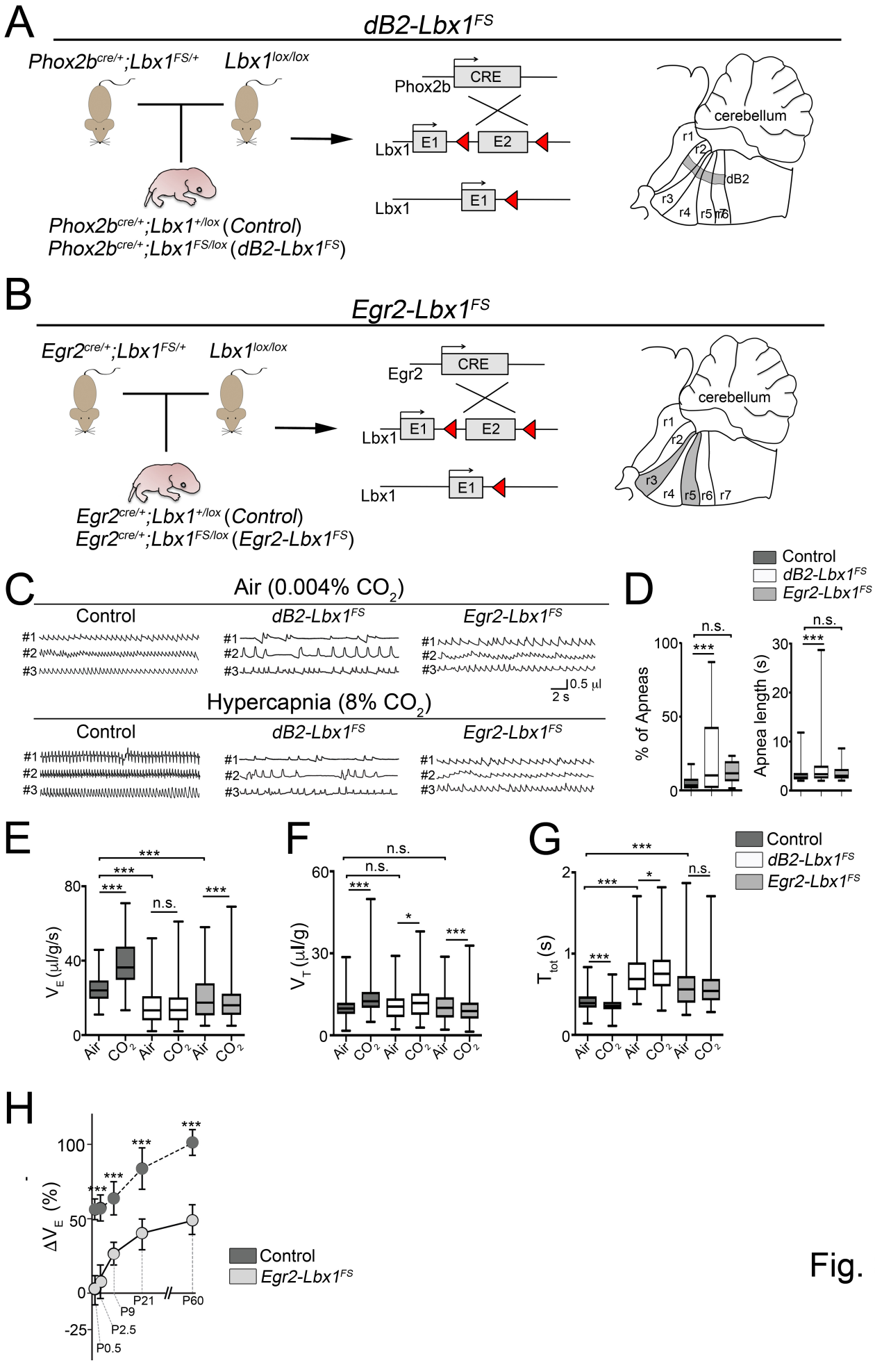
A
dB2-Lbx1FS
Phox2bcre/+;Lbx1FS/+
Lbx1lox/lox
Phox2b
CRE
Lbx1
E1
E2
cerebellum
r1
r2
dB2
r3
r4
r5
r6
Phox2bcre/+;Lbx1+/lox (Control)
Phox2bcre/+;Lbx1FS/lox (dB2-Lbx1FS)
B
Egr2-Lbx1FS
Egr2cre/+;Lbx1FS/+
Lbx1lox/lox
Egr2
CRE
Lbx1
E1
E2
cerebellum
r1
r2
r3
r4
r5
r6
r7
Egr2cre/+;Lbx1+/lox (Control)
Egr2cre/+;Lbx1FS/lox (Egr2-Lbx1FS)
C
Air (0.004% CO2)
Control
dB2-Lbx1FS
Egr2-Lbx1FS
#1
#2
#3
0.5 µl
2 s
Hypercapnia (8% CO2)
Control
dB2-Lbx1FS
Egr2-Lbx1FS
#1
#2
#3
D
Control
dB2-Lbx1FS
Egr2-Lbx1FS
% of Apneas
Apnea length (s)
n.s.
***
E
VE (µl/g/s)
F
VT (µl/g)
G
Ttot (s)
Control
dB2-Lbx1FS
Egr2-Lbx1FS
n.s.
*
***
Air
CO2
H
ΔVE (%)
P0.5
P2.5
P9
P21
P60
Control
Egr2-Lbx1FS

Fig. S6

Fig. S6. Conditional genetic strategies to restrict the *Lbx1*^{FS} mutation to specific neuronal subpopulations. (**A,B**) Genetic strategies to restrict the *Lbx1*^{FS} mutation to the dB2 lineage and to rhombomere 3 and 5 (rhombomer 5 is the origin of RTN neurons). The *Lbx1*^{lox} allele contains LoxP sites (red triangles) flanking exon 2 of the Lbx1 locus. (**A**) Cre-mediated recombination of the *Lbx1*^{lox} allele in *dB2-Lbx1*^{FS} mutants produced a *Δ/FS* mutation in cells with a history of Phox2b expression, i.e. cells of the dB2 lineage (indicated in gray in the scheme on the right). (**B**) Cre-mediated recombination of the *Lbx1*^{lox} allele in *Erg2-Lbx1*^{FS} mutants produced a *Δ/FS* mutation in cells with a history of Egr2 expression, i.e. cells of rhombomeres 3 and 5 (indicated in gray in the scheme on the right). (**C-G**) Breathing analysis of control (n=20), *dB2-Lbx1*^{FS} (n=11) and *Egr2-Lbx1*^{FS} (n=12) mice at birth. (**C**) Representative plethysmographic traces of control, *dB2-Lbx1*^{FS} and *Egr2-Lbx1*^{FS} newborns in normal air (0.04% CO_2) and high CO_2 containing air (hypercapnia, 8% CO_2). Numbers on the left of the traces indicate individual animals tested. (**D**) **(**Left) Quantification of the percentage of apneic episodes (per 5-minute breathing recordings; unpaired non-parametric Mann-Whitney U test). (Right) Quantification of apnea lengths (per 5-minute breathing recordings; unpaired non-parametric Mann-Whitney U test). (**E**) Quantification of ventilatory minute volumes (V_E) of control, *dB2-Lbx1*^{FS} and *Egr2-Lbx1*^{FS} newborn mice in normal air and high CO_2 containing air (unpaired non-parametric Mann-Whitney U test). (**F**) Quantification of tidal volumes (V_T; unpaired non-parametric Mann-Whitney U test) of control, *dB2-Lbx1*^{FS} and *Egr2-Lbx1*^{FS} newborns in normal air and in high CO_2 containing air. (**G**) Quantification of breath cycle

duration (T_{TOT}; unpaired non-parametric Mann-Whitney U test) of control, *dB2-Lbx1^{FS}* and *Egr2-Lbx1^{FS}* newborns in normal air and in high CO_2 containing air. (**H**) Analysis of the response to hypercapnia; change (Δ) of ventilatory minute volumes (V_E) in control and *Egr2-Lbx1^{FS}* mice at different time points. *P< 0.01; ***P < 0.0001.

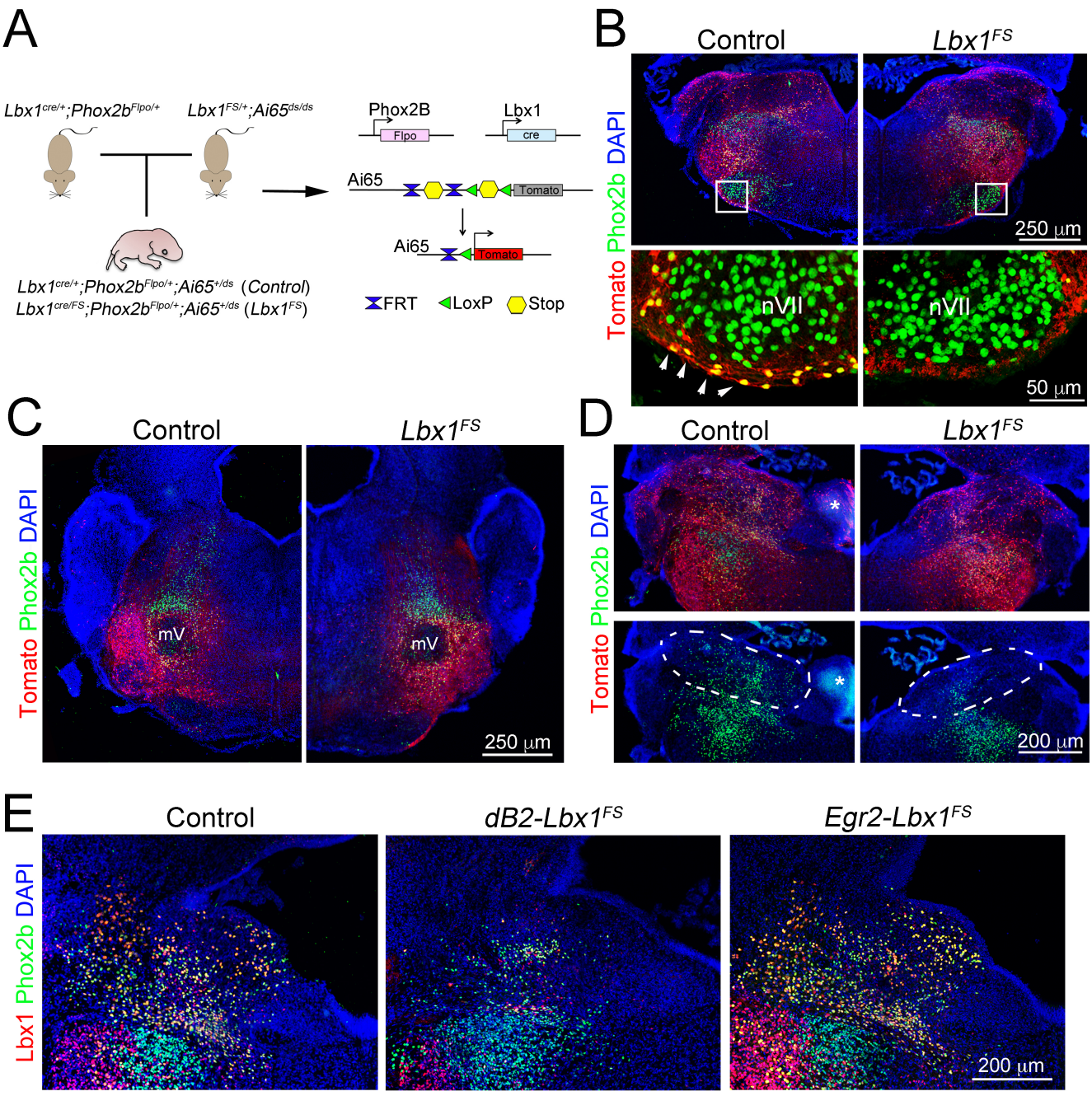
A
Lbx1cre/+;Phox2bFlpo/+
Lbx1FS/+;Ai65ds/ds
Phox2B
Flpo
Lbx1
cre
Ai65
Tomato
Ai65
Tomato
Lbx1cre/+;Phox2bFlpo/+;Ai65+/ds (Control)
Lbx1cre/FS;Phox2bFlpo/+;Ai65+/ds (Lbx1FS)
FRT
LoxP
Stop
B
Control
Lbx1FS
Tomato Phox2b DAPI
nVII
nVII
250 μm
50 μm
C
Control
Lbx1FS
Tomato Phox2b DAPI
mV
mV
250 μm
D
Control
Lbx1FS
Tomato Phox2b DAPI
*
*
200 μm
E
Control
dB2-Lbx1FS
Egr2-Lbx1FS
Lbx1 Phox2b DAPI
200 μm

Fig. S7

Fig. S7. Intersectional genetic labeling of dB2 neurons in control and *Lbx1^{FS}* mice. (**A**) Schemes illustrating the genetic strategy to label dB2 neurons with Tomato fluorescent protein using intersectional recombination. Cre and a Flpo recombinases were driven by Lbx1 and Phox2b (*Lbx1$^{cre/+}$;Phox2b$^{Flpo/+}$*) to remove the double stop (ds) cassettes present in the *Ai65* indicator line. Tomato fluorescent protein is expressed after dual recombination. (**B-D**) Histological analysis of Tomato+ (red) dB2 neurons counterstained with Phox2b antibodies (green) in control and *Lbx1^{FS}* newborn mice. DAPI (blue) was used as counterstain. Confocal tile scan modus was used to acquire photomicrographs, and assembled using ZEN2012 software (10% overlap between tiles). (**B**) Tomato+/Phox2b+ RTN neurons (arrowheads in lower panels). The lower panels show a magnification of the boxed areas. (**C**) Tomato+/Phox2b+ peri-V neurons locate around the trigeminal motor (mV) nucleus. (**D**) (Upper panels) Dorsal Tomato+/Phox2b+ neurons at the level of rhombomere 5. The Tomato+/Phox2b+ neuronal population was observed across rhombomere 3-6. (Lower panels) For a better visualization of dorsal Phox2b+ neurons (dashed area), the Tomato+ signal was removed. Note the severe reduction in the number of Phox2b+ neurons in *Lbx1^{FS}* mice. (**E**) Comparison of the dorsal Phox2b+ (green) neuronal population co-stained with Lbx1 (red) antibodies in control, *dB2-Lbx1^{FS}* and *Egr2-Lbx1^{FS}* newborn mice. The quantification of RTN, periV and the dorsal Lbx1+/Phox2b+ neurons in control, *Lbx1^{FS}*, *dB2-Lbx1$^{FS/FS}$* and *Egr2-Lbx1^{FS}* is presented in Fig. 4B.

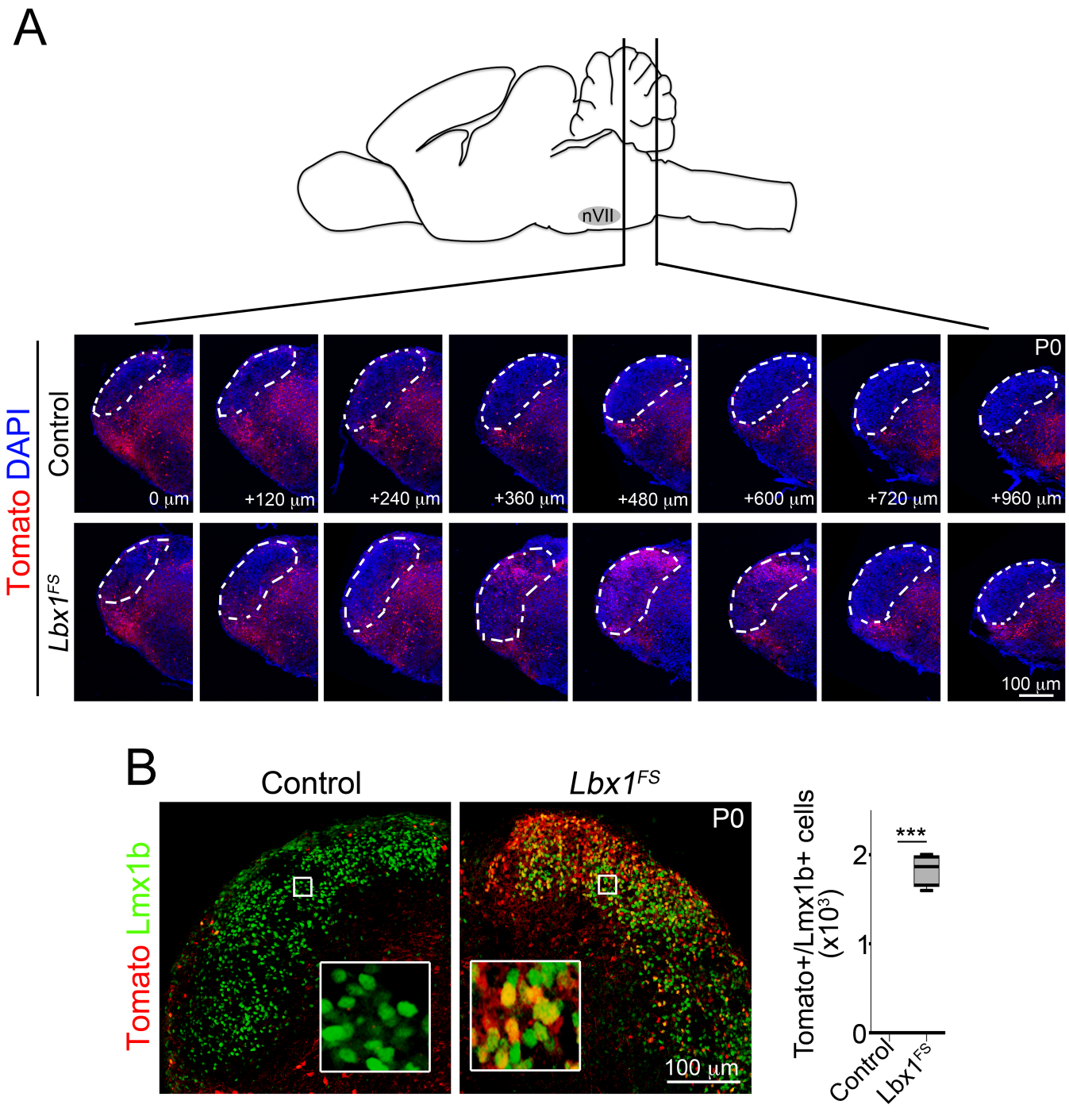
A
nVII
Tomato DAPI
Control
Lbx1FS
0 µm
+120 µm
+240 µm
+360 µm
+480 µm
+600 µm
+720 µm
+960 µm
P0
100 µm
B
Control
Lbx1FS
Tomato Lmx1b
P0
100 µm
Tomato+/Lmx1b+ cells (x10³)
***
2
1
0
Control
Lbx1FS

Fig. S8

Fig. S8. Ectopic dB2-derived neurons in the dorsal spinal trigeminal nucleus of *Lbx1^{FS}* mice. (**A**) (Upper panel) Scheme illustrating the section planes used to identify Tomato+ dB2 neurons in the caudal hindbrain of control and *Lbx1^{FS}* newborn mice (see Supplementary Fig. 6a for a scheme of the genetic strategy). The caudal apex of the facial motor (nVII) nucleus was considered as position 0, and consecutive sections spaced every 120μm were analyzed. DAPI (blue) was used for a counterstain. (**B**) Histological analysis and quantification of Tomato+ (red) neurons in the dorsal spinal trigeminal nucleus co-expressing the somatosensory marker Lmx1b (green) in control (n=3) *Lbx1^{FS}* (n=3) mice (unpaired t test, t=19,49 df=6). Boxed areas are magnified in the insets. ***p<0.0001. Confocal tile scan modus was used to acquire photomicrographs, and assembled using ZEN2012 software (10% overlap between tiles).

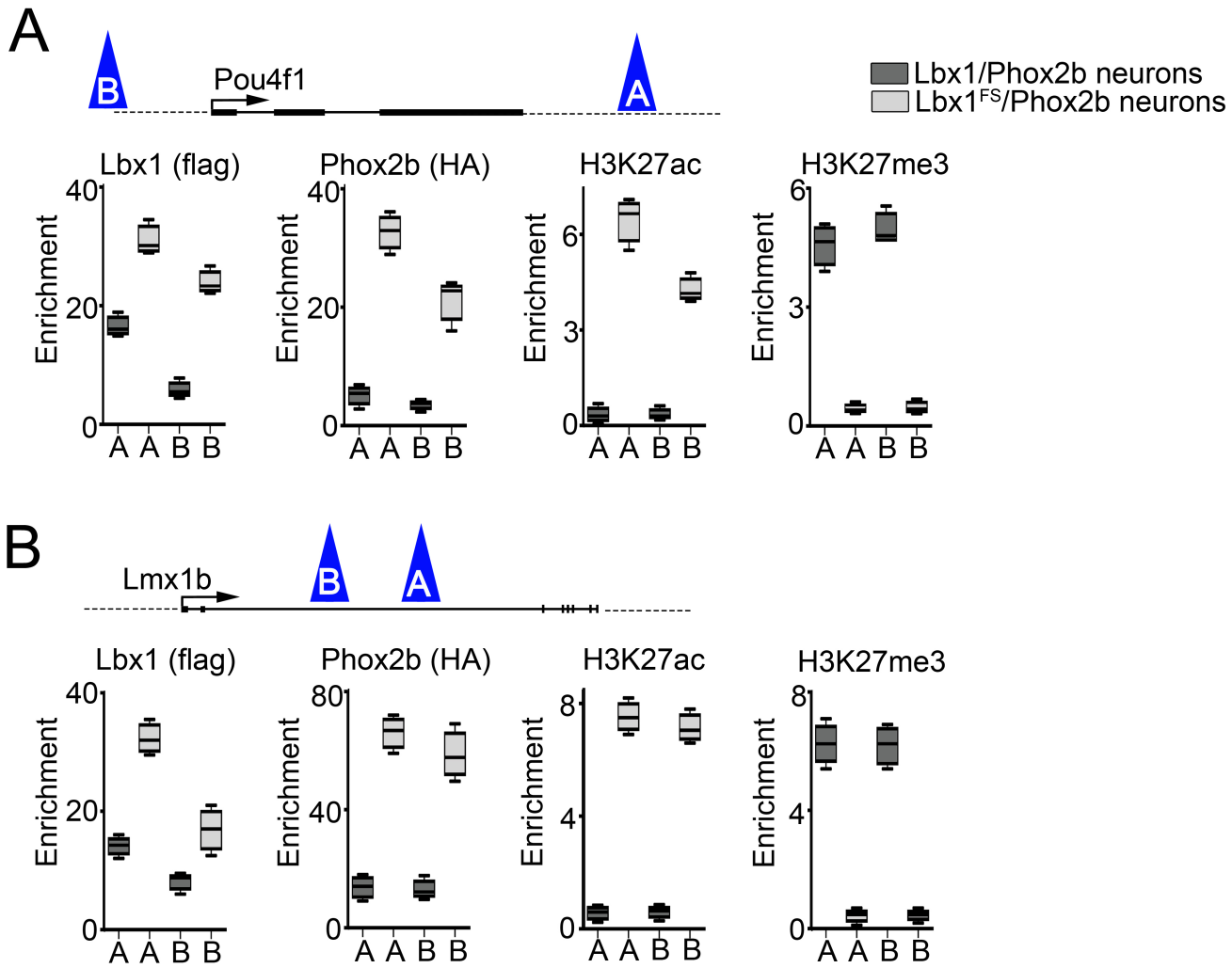
A
B
Pou4f1
A
Lbx1/Phox2b neurons
Lbx1FS/Phox2b neurons
Lbx1 (flag)
Phox2b (HA)
H3K27ac
H3K27me3
Enrichment
A A B B
B
Lmx1b
B
A
Lbx1 (flag)
Phox2b (HA)
H3K27ac
H3K27me3
Enrichment
A A B B

Fig. S9

Fig. S9. Enhancer analysis of somatosensory genes in Lbx1/Phox2b and Lbx1^{FS}/Phox2b neurons. (A, B) ChIP-qPCR analysis performed on chromatin prepared from Lbx1/Phox2b and Lbx1^{FS}/Phox2b expressing neurons using antibodies that detect flag-tag (for Lbx1 and Lbx1^{FS} immunoprecipitation, n=4 independent replicates), HA-tag (for Phox2b immunoprecipitation, n=4 independent replicates), H3K27ac (n=4 independent replicates) and H3K27me3 (n=4 independent replicates). Analyzed sites in the *Pou4f1* (**A**) and *Lmx1b* (**B**) loci are indicated schematically; blue triangles represent enhancers bound by Lbx1 and Lbx1^{FS} (see SI Appendix, Fig. S2A).

Supplementary Table 1. Primer and Oligo sequences used in this study

Oligo sequences to mutate Lbx1 in P19 cells

Name	Sequence 5'-3'
sgRNA guide 1 Forward	CCTTCCTCTCGCACCGTCCA
sgRNA guide 1 Reverse	CTCACAGAGTGCAAGGAAACCACA
sgRNA guide 2 Forward	TGGGGTCTTGACTCTCTCGT
sgRNA guide 2 Reverse	CCATACAGAATTGCACGGCGAGG

Primer sequences to analyze Lmx1b, Prrxl1, Pou4f1 and Lbx1 expression in P19 cells

Name	Sequence 5'-3'
Lmx1b-F	AAAGACCCGAGAAGGCCCAA
Lmx1b-R	CTCCATGGCCACGATCTGCT
Prrxl1-F	CTGAACACAGCCACGTATGCC
Prrxl1-R	ACTCTTCTCTCCCTCGCTCT
Pou4f1-F	ACCATCTGCAGGTTCGAGTC
Pou4f1-R	TTTCATCCGCTTCTGCTTCT
Lbx1-F	ATCTTCCTGCATTTTCTCGGACT
Lbx1-R	ACAGACGGACCCAGAGCTAC
Tbp-F (housekeeping)	CCCCACAACTCTTCCATTCT
Tbp-R (housekeeping)	GCAGGAGTGATAGGGGTCAT
b-actin-F (housekeeping)	AGCAGTTGGTTGGAGCAAACATCC
b-actin-R (housekeeping)	ACAGAAGCAATGCTGTCACCTTCC

Primer sequences to analyze Lmx1b, Prrxl1 and Pou4f1 enhancers

Name	Sequence 5'-3'	Peak coordinates
Lmx1b-A-F	CCTTCACTGCTTCGTCT	(mm9) chr2:33460946-33461331
Lmx1b-A-R	TAATTACGGAGTGCAGAACCC	(mm9) chr2:33460946-33461331
Lmx1b-B-F	TCTCTTGTTGGCCCGTTTAGTGG	(mm9) chr2:33436176-33436518
Lmx1b-B-R	AGCTTCCTCAATAATCGCTCT	(mm9) chr2:33436176-33436518
Lmx1b-CA-F	GGCATCAAATGACAGGA	(mm9) chr2:33489220-33489682
Lmx1b-CA-R	TTTAGCGCTCTACAGTT	(mm9) chr2:33489220-33489682
Pou4f1-B-F	TGCAGCCCCTAATAAATCCAG	(mm9) chr14:104854146-104854519
Pou4f1-B-R	CAGCACAGTAATTAAACTAGCAA	(mm9) chr14:104854146-104854519
Pou4f1-A-F	TAAAACTGCAGGGGGAACTG	(mm9) chr14:104936831-104937434
Pou4f1-A-R	CCCAAAGATCAGGGAACAGA	(mm9) chr14:104936831-104937434
Pou4f1-CA-F	TAAGGTGGTCAATCCTGT	(mm9) chr14:104880386-104880946
Pou4f1-CA-R	TTGAGCCACTTATAGAGGATG	(mm9) chr14:104880386-104880946
Prrxl1-A-F	TCCCTTTGCTATGGACTTGG	(mm9) chr14:33452910-33453370
Prrxl1-A-R	CACTCCAAAAGCATCCCACT	(mm9) chr14:33452910-33453370
Prrxl1-B-F	CCACTTCCCTTTGCTATGGA	(mm9) chr14:33452938-33453358
Prrxl1-B-R	CACTCCAAAAGCATCCCACT	(mm9) chr14:33452938-33453358
Prrxl1-CA-F	CCTGTGGCCATGAAACACC	(mm9) chr14:33446510-33447239
Prrxl1-CA-R	AGAAAACGCAGGTCCAGT	mm9) chr14:33446510-33447239